Short excitonic lifetimes of $MoSe_2$ monolayers grown by molecular beam epitaxy on the hexagonal boron nitride

2D Materials

OPEN ACCESS

RECEIVED
24 October 2023

REVISED
27 January 2024

ACCEPTED FOR PUBLICATION
7 March 2024

PUBLISHED
15 March 2024

PAPER

Short excitonic lifetimes of $MoSe_2$ monolayers grown by molecular beam epitaxy on the hexagonal boron nitride

Kacper Oreszczuk[1,*], Wojciech Pacuski[1], Aleksander Rodek[1], Mateusz Raczyński[1], Tomasz Kazimierczuk[1], Karol Nogajewski[1], Takashi Taniguchi[2], Kenji Watanabe[3], Marek Potemski[1,4,5] and Piotr Kossacki[1]

[1] Institute of Experimental Physics, Faculty of Physics, University of Warsaw, Pasteura 5, Warsaw 02-093, Poland
[2] Research Center for Materials Nanoarchitectonics, National Institute for Materials Science, 1-1 Namiki, Tsukuba 305-0044, Japan
[3] Research Center for Electronic and Optical Materials, National Institute for Materials Science, 1-1 Namiki, Tsukuba 305-0044, Japan
[4] Laboratoire National des Champs Magnétiques Intenses, UPR 3228, CNRS, EMFL, Univ; Grenoble Alpes, Grenoble 38042, France
[5] CENTERA Labs, Institute of High Pressure Physics, PAS, Warsaw 01-142, Poland
[*] Author to whom any correspondence should be addressed.

E-mail: Kacper.Oreszczuk@fuw.edu.pl

Keywords: molecular beam epitaxy, $MoSe_2$, transition metal dichalcogenides, time resolved photoluminescence, excitation correlation spectroscopy, excitonic lifetimes

Supplementary material for this article is available online

Abstract

We present a time-resolved optical study of recently developed narrow-line $MoSe_2$ monolayers grown on hexagonal boron nitride with means of molecular beam epitaxy. We find that the photoluminescence decay times are significantly shorter than in the case of the exfoliated samples, even below one picosecond. Such a short timescale requires measurements with better resolution than achievable with a streak camera. Therefore, we employ an excitation correlation spectroscopy pump-probe technique. This approach allows us to identify two distinct non-radiative recombination channels attributed to lattice imperfections. The first channel is active at helium temperatures. It reduces the lifetime of the neutral exciton to below one picosecond. The second channel becomes active at elevated temperatures, further shortening the lifetimes of both neutral and charged exciton. The high effectiveness of both radiative and non-radiative recombination makes epitaxial $MoSe_2$ a promising material for ultrafast optoelectronics.

1. Introduction

Monolayers of transition metal dichalcogenides (TMDs) draw a lot of attention as semiconducting materials with robust optical properties, strong Coulomb interaction [1–3] and an optically accessible valley degree of freedom [4–7]. The extraordinary properties of TMDs make them promising candidates for applications in photonics and optoelectronics. Fundamental research on such systems usually required using exfoliated or mechanically transferred layers, as they provided the best optical properties, in particular: narrow linewidths of excitonic transitions [8–11]. The exfoliation process, however, suffers from limited scalability and large inhomogeneity, hindering the perspectives of potential commercial applications.

Epitaxial techniques, such as molecular beam epitaxy (MBE), are advantageous as they eliminate the aforementioned drawbacks: they provide reproducible, wafer-scale, homogeneous layers [12–14]. However, for a long time, epitaxial techniques suffered from significant spectral broadening, which hindered the observation of various interesting optical effects. Fortunately, a recent report [15] has addressed this issue by implementing slow-growth-rate epitaxy on an atomically flat hexagonal boron nitride substrate. This novel approach has enabled the growth of excitonic narrow line MBE $MoSe_2$ monolayers, thereby opening up possibilities for advanced, time-resolved optical research, as demonstrated in this manuscript.

Short excitonic lifetimes and relaxation times observed in monolayers of semiconducting TMDs [16–21] are promising for applications in nonlinear optics [22, 23] that may now become viable due to the development of scalable growth process of high optical quality material [15, 24]. Possible applications

include higher harmonic generation [25, 26], THz wave generation [27, 28], parametric amplification [29] or nanoscale light sources [29, 30]. Such processes require control over the characteristic times of the excitonic relaxation processes. In this work, we employ various experimental approaches to investigate the excitonic dynamics in epitaxially grown $MoSe_2$ monolayer quantitatively, and we observe relaxation, which is even faster than in the case of exfoliated TMD layers.

2. Methods

The epitaxial growth of studied $MoSe_2$ was made possible by employing the hexagonal boron nitride substrate. Thin hBN flakes obtained by mechanical exfoliation were deposited on a silicon substrate with a layer of silicon oxide with a thickness of 90 nm. Prepared substrates were placed in the chamber of the molecular beam epitaxy machine, where $MoSe_2$ was grown over the entire surface of the sample (figures 1(b) and (c)). The growth was performed at the temperature of 300 °C and was followed with high-temperature annealing in the temperature of 750 °C. Such a procedure allowed us to obtain a high-quality monolayer with relatively small areas where $MoSe_2$ is discontinuous or takes the form of a bilayer (figures 1(b) and (c)). Two samples were grown in separate growth processes for experiments described in this work. The sample used in the first part of this work (figures 1–4) was grown with a very slow growth rate (10 h Ml^{-1}), while the second sample (figures 5 and 6) was grown with a moderate growth rate (25 min Ml^{-1}). More details of the growth process are described in [15, 31].

Optical measurements were carried out in a helium bath cryostat. Samples were placed in a gaseous helium atmosphere at the temperature of 5 K, unless noted otherwise. The laser beam was focused by a single aspheric lens (numerical aperture = 0.68) to a spot smaller than 2 μm. The sample was mounted on the x–y–z piezoelectric stage inside the cryostat.

Time-resolved measurements were performed with a pulsed OPO laser tuned at 610 nm (2030 meV). The repetition rate was 75.7 MHz with a half-maximum pulse width of 160 fs. The streak camera measurements were performed with averaged laser power equal to 100 μW.

A large part of the time-resolved measurements was performed with excitation correlation spectroscopy (ECS) technique [32, 33]. In ECS measurement, the time-integrated PL spectrum is acquired under the excitation from two identical laser pulse trains. The total PL intensity of excitonic peaks is probed for different delays between the pulse trains. ECS measurement is effective if the dependence of the PL intensity on the excitation power is not linear. We consider the simplified model of saturation behavior related to the limited poll of the unoccupied excitonic states. Under such a picture, the number of excitons created with individual laser pulse is proportional to the number of unoccupied excitonic states at the time of the impact. The PL intensity reaches a minimum when the laser pulses overlap temporarily. If the pulses are separated, the PL intensity rises exponentially with the delay between pulses, asymptotically reaching its large-separation limit. The characteristic time of this exponential behavior is assumed to be exactly equal to the population lifetime of the studied excitonic state.

Other causes of the sublinearity at the excitation mechanism may include, for example, the Auger recombination. In this case, the ECS signal decay is generally faster than the population decay. The difference, however, would only be significant in the regime of the very high excitation powers, where the higher-order components in the ECS transient emerge. See supplementary infomation for a more detailed exploration of the scope and applicability of the ECS approach in the presence of the Auger recombination.

Regardless of the exact mechanism behind the ECS transients, we interpret the ECS characteristic times as related to the respective excitonic lifetimes. We estimate that in this work, the population lifetimes are underestimated by no more than 20%, even if the Auger recombination was the only source of the sublinearity at the excitation mechanism.

ECS measurements were carried out with two identical laser pulse trains, each at the average laser power of 120 μW . The time separation between pulses was tuned with a delay line.

3. Results

The photoluminescence decay transients of the neutral and negatively charged excitons (X, CX) measured directly with a streak camera are presented in figure 2. The measurement reveals the short main component of the photoluminescence decay, followed by the weaker long-lived signal. The lifetimes of the short components are significantly smaller compared to the exfoliated samples presented in literature [34, 35] and in the supplementary information of this work. The typical photoluminescence lifetime in exfoliated $MoSe_2$ monolayers is between 2 ps and 10 ps for the neutral exciton and between 5 ps and 100 ps for the charged exciton.

To quantify the observed decay times, we fit the biexponential decay:

$$I(t) = \frac{A}{\tau}\exp\left(-\frac{t}{\tau}\right) + \frac{B}{\tau_{\text{long}}}\exp\left(-\frac{t}{\tau_{\text{long}}}\right). \quad (1)$$

The fits were performed in convolution with the impulse response function of the experimental setup, which was approximated with a Gaussian transient corresponding to the experimentally obtained laser pulse profile.

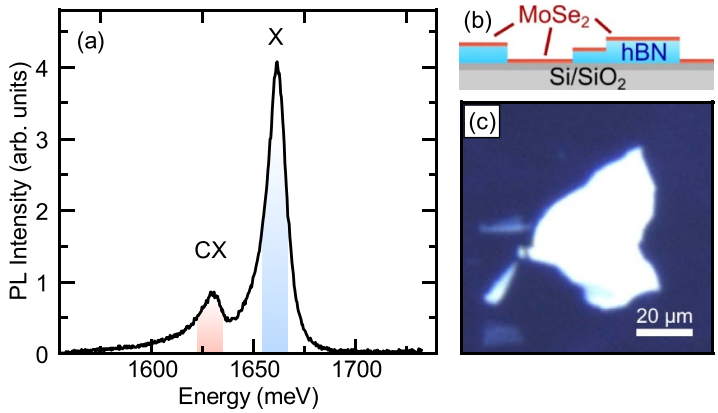

Figure 1. (a) Normalized PL spectra of the MBE $MoSe_2$ monolayer on hBN flake under the pulsed excitation with 610 nm (2030 meV), 120 μW laser. The shaded regions span the spectral integration range for X and CX peaks during the time-resolved measurements. (b) Scheme of the $MoSe_2$ monolayer grown on Si/SiO_2 substrate partially covered with hBN flakes. (c) Photograph of the example hBN flake covered with $MoSe_2$ monolayer.

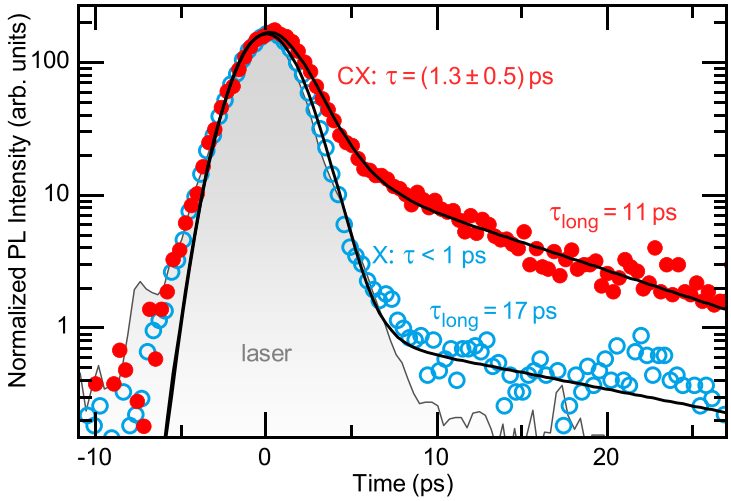

Figure 2. Time-resolved PL of neutral (open symbols) and charged (closed symbols) exciton peaks obtained with the streak camera, at $T = 5$ K for epitaxial $MoSe_2$ monolayer grown on hBN. Solid black lines: fit of the double-exponential decay of charged exciton convoluted with impulse response function approximated by Gaussian. The impulse Response Function of the experimental setup, as measured on the laser pulse, is presented as a grey area.

The lifetime τ of the short-lived component of the PL signal is below the resolution of the streak camera, allowing only for its course estimations. We observe the lifetime of X resonance to be shorter than 1 ps, and the lifetime of the CX resonance being in the order of 1.3 ps. Weak, long-lived components of the lifetime of 10–20 ps may be related to excitons localized on charge fluctuations, nonuniform strain, or defects. Such localizing centers may be more abundant in MBE-grown samples considering their richer microscopic structure [15, 36]. The long component is spectrally correlated with the neutral and charge exciton photoluminescence signal and is characterized by a common timescale for both excitonic peaks, which can be a fingerprint of a long-lived reservoir higher in the relaxation ladder exposed in conditions of non-resonant excitation.

Quantitative investigation of processes in subpicosecond timescale requires an experimental method capable of higher temporal resolution than provided by a streak camera. Hence, we employ the ECS technique, which provides a time resolution comparable to the width of the laser pulse. The result of the example ECS measurement is presented in figure 3. The PL intensity from the $MoSe_2$ is integrated over the spectral ranges of X and CX resonances (See: figure 1(a) and probed with different time delays between two laser pulse trains. Similarly, as in the case of the Streak Camera measurements, two-exponential decay of the signal is observed. The laser autocorrelation function of FWHM = 260 ps (corresponding to the pulse duration of 180 ps) was used as an impulse response function during fitting. The characteristic times of the fast component of the ECS signal are

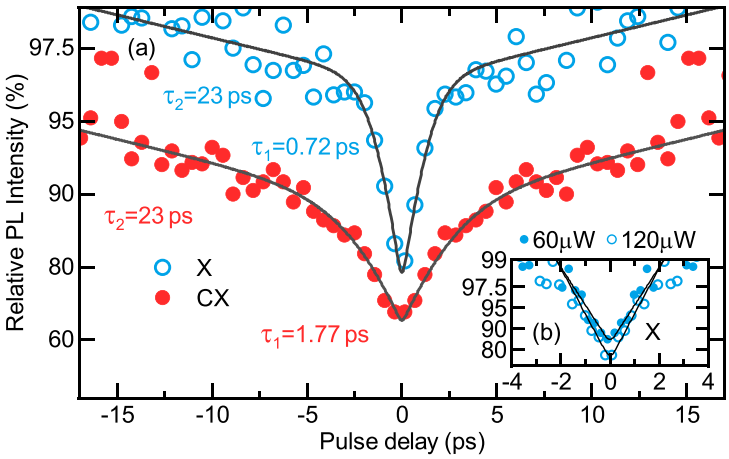

Figure 3. CS signal of neutral and charged exciton peaks at the temperature of 5 K, measurd for epitaxial $MoSe_2$ monolayer grown on hBN. PL intensity is normalized to the limit of infinite pulse separation. Inset: ECS signal acquired under two different excitation powers. The long-lived component was subtracted for clarity. Values of 60 μW and 120 μW relate to the power of the individual pulse train.

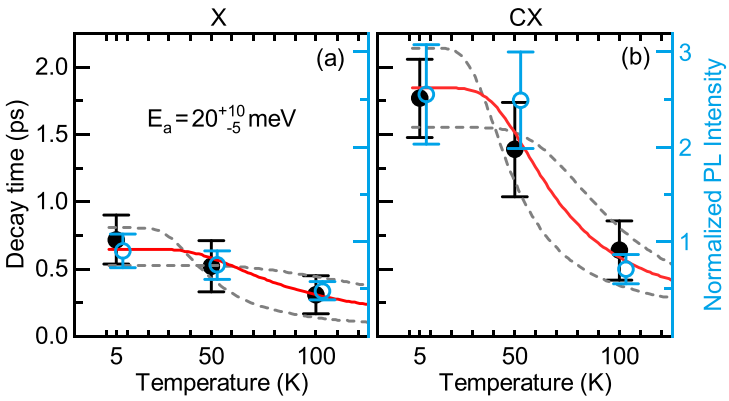

Figure 4. Comparison of (a) neutral and (b) charged exciton ECS signal decay times (solid markers) with their total PL intensity (open markers, slightly shifted for clarity) presented as a function of temperature. The vertical scale of PL Intensity was normalized on each panel to match the ECS signal decay times on the opposite vertical axis. Lines—fits of the Arrhenius equation with activation energy parameters: $E_a = 20$ meV (solid line), $E_a = 15$ meV, $E_a = 30$ meV (dashed lines).

equal to 0.72 ps for X resonance, and 1.77 ps for CX resonance (figure 3). These values are in quantitative agreement with the direct measurements of the PL decay time. We observe little dependence on the excitation power (inset in figure 3), which proves that observed ECS transients are directly related to the exciton lifetimes. No fingerprints of the carrier relaxation between the optical excitation and PL emission energies were observed. We estimate that such relaxation processes occur in timescales shorter than 200 ps. See supplementary infomation, chapter 4 for an extended discussion of the role of delayed exciton formation.

Measured excitonic lifetimes were similar for samples grown in different conditions and regardless of their degree of degradation in environmental conditions (supplementary information, figure 2). This suggests that the nature of the extraordinarily short excitonic lifetimes is directly related to the epitaxial growth process. Chalcogenide vacancies are the most prevalent defect site in exfoliated samples [37]. Non-equilibrium epitaxial growth in high vacuum further increases the prevalence of the selenium vacancies [36], which may be the dominant contributor to the observed rapid decay.

Having established a suitable tool that allows for probing of the short excitonic lifetimes, we investigate the temperature's effects on the recombination dynamics. The increase of the temperature results in further shortening of the decay time obtained for X and CX peak (figures 4(a) and (b)). The shortening is followed by a proportional decrease of the total intensity of the luminescence signal. The long-lived component can be neglected, as it composes under 10% of the total photoluminescence intensity (figure 2).

The correlation between the lifetime and the total intensity evidences strong thermally-activated non-radiative recombination channels. We model the excitonic recombination rates with the

low-temperature component τ_0^{-1} and additional, thermally activated component described by the Arrhenius equation:

$$\tau^{-1} = \tau_0^{-1} + A \exp \frac{-E_a}{k_B T}. \quad (2)$$

We fit the Arrhenius equation to the experimental data in figures 4(a) and (b) and obtain the activation energy of the non-radiative processes equal to $E_a = 20^{+10}_{-5}$ meV. The same value of E_a was used for X and CX fits in figures 4(a) and (b).

The microscopic structure of the monolayer is characterized by abundant gaps or bilayer fragments [15]. With the relatively high point defect density [36] and the average distance to the monolayer edge in the ballpark of tens of nanometers, the transport effects can be relevant to the efficiency of the recombination channels. The diffusion coefficient and the mean free time are relatively high in monolayer $MoSe_2$ [38], allowing efficient transport over tens of nanometers in subpicosecond timescale. The decrease of the excitonic lifetime in elevated temperatures may result from increased carrier mobility towards the monolayer edges or areas of increased point defect density. In this interpretation, the activation energy of $E_a = 20^{+10}_{-5}$ meV is related to the amplitude of the potential fluctuations in the sample plane. The linewidths of the excitonic transitions are significantly smaller than the activation energy, which indicates a high degree of exciton localization.

Next, we investigate the recombination processes at low temperatures below the activation threshold. The low-temperature excitonic recombination rate τ_0^{-1} can be described as a sum of the radiative (τ_γ^{-1}) and non-radiative (τ_{NR}^{-1}) terms:

$$\tau_0^{-1} = \tau_\gamma^{-1} + \tau_{NR}^{-1}. \quad (3)$$

The radiative decay rate is expected to depend strongly on the thickness of the hBN bottom layer due to the Purcell effect [35]. Assuming that the non-radiative effects remain unchanged regardless of the photonic environment, it is possible to determine whether radiative or non-radiative channels are a dominant recombination mechanism at low temperatures.

Figure 5(a) shows the reflectivity spectra of four $MoSe_2$ monolayers grown simultaneously on different hBN flakes. The thickness of the flakes was obtained from the reflectivity measurements in a broad VIS-NIR range. The spectra were fitted with the dispersion-corrected refractive indexes of the hBN and SiO_2 (90 nm) layers. Having determined the thicknesses of the hBN, we calculated the Purcell factors for the excitonic emission. Two selected spots were characterized by the low Purcell factor of 0.26 and 0.30, while the other two exhibited high values of 0.93 and 1.21. The Purcell factor F_p was calculated in line with equations (S35)–(S38) in the supplementary information of the related work of Fang *et al* [35].

The time-resolved profiles of the ECS signal were acquired at each studied spot (figures 5(b)–(e)). We find that the dynamics of the ECS signal are not significantly dependent on the calculated Purcell factor. The calculated decay times of X and CX peaks were equal to about 0.65 ps and 2.0 ps, respectively, similar to the results obtained on the other sample at the temperature of 5 K. Any variations between spots of different Purcell factors were confined within the experimental uncertainty, which suggests a dominant role of the non-radiative excitation channels even at low temperatures.

The dependence of the decay times of the X and CX peaks on the Purcell Factor is presented on figure 6. Based on the acquired data we provide estimations on the radiative and non-radiative recombination terms. Lower boundary estimation of the characteristic time of the non-radiative processes can be obtained under the assumption of negligible (but sufficient to observe the PL signal) relative efficiency of the radiative processes. We estimate the τ_{NR}^{X} to be greater than 0.5 ps and τ_{NR}^{CX} to be greater than 1.6 ps. In the alternate edge case of relatively strong radiative recombination, we estimate the upper limit of the τ_{NR}^{X} to be 1.1 ps and the upper limit of the τ_{NR}^{CX} to be 2.7 ps. Presented estimations result in the radiative recombination times in all cases equal to 1.25 ps or greater for the neutral exciton and 8 ps or greater for the charged exciton (at the Purcell factor of $F_P = 1$). The above ranges result in upper limits of quantum efficiency of photoluminescence of 0.47 for X and 0.25 for CX (at $F_P = 1$).

4. Discussion

We show that MBE-grown $MoSe_2$ gives stable and high optical quality photoluminescence that facilitates the application of advanced time-resolved spectroscopy techniques. The observed excitonic lifetimes remain similar in different spots on the sample as well as on two independently grown samples, proving uniformity, reliability, and the repeatability of the growth process. The excellent performance of our samples draws closer to the perspective of substituting exfoliated flakes with an industrially scalable alternative in a broad range of potential applications, particularly after the use of epitaxial hBN substrate [24].

We observe that the PL decay times of MBE-grown monolayers are significantly shorter than in the typical exfoliated samples. Utilizing the ECS technique, we identified two independent non-radiative recombination channels responsible for the shortening of the excitonic lifetimes. One in low temperatures was identified by probing monolayers in photonic environments described by different Purcell Factors. The non-radiative recombination at low temperatures dominates over the radiative channel, and

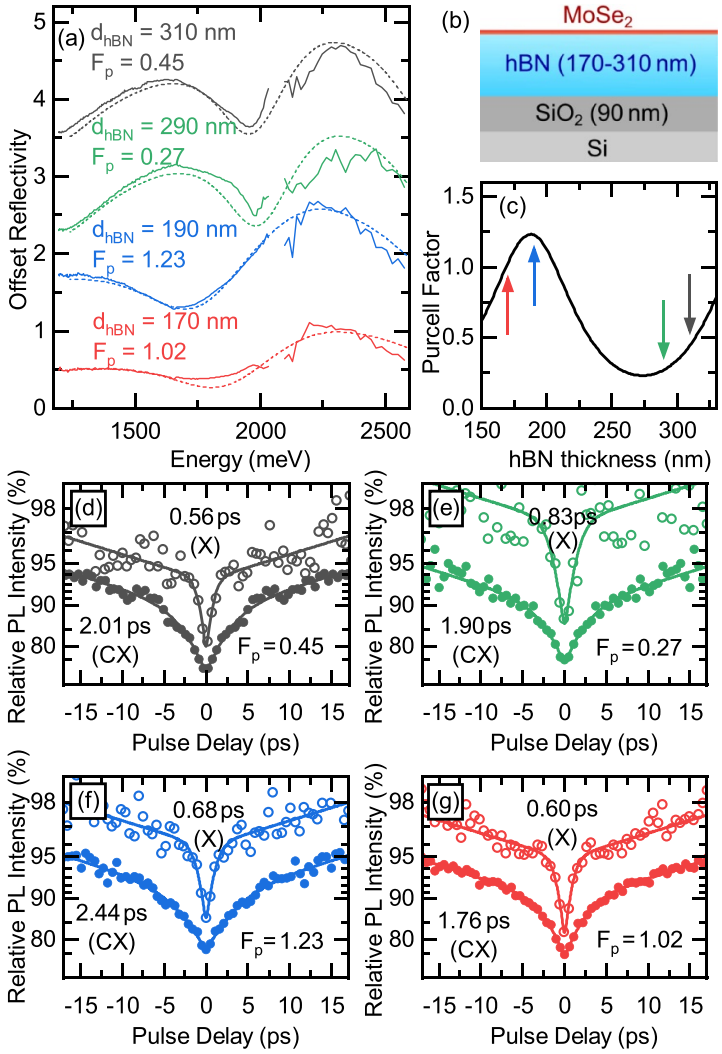

Figure 5. (a) Solid lines: reflectivity spectra of the $MoSe_2$ monolayer grown on the hBN flakes of varying thickness. Dashed lines: simulation result used for calculation of the gBN thickness. (b) Schematic representation of the sample structure (c) Predicted Purcell Factor at different thicknesses of the hBN spacer. (d)–(g) Time-resolved measurements of the ECS signal decay for X and CX on spots on the sample with low (d)–(e) and high (f)–(g) predicted values of the Purcell factor.

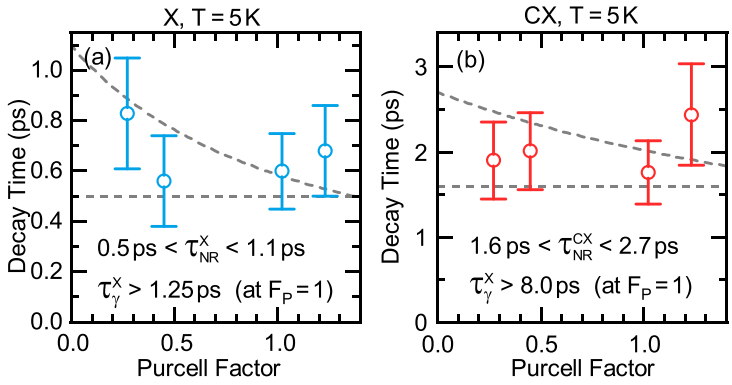

Figure 6. Characteristic decay times of neutral (a) and charged (b) exciton on the spots with different Purcell factors. Gray lines: fits for low and high estimates of the characteristic time of the non-radiative recombination channels.

can be attributed to the high density of selenium vacancies resulting from the epitaxial growth process. It brings the neutral exciton lifetime from several picoseconds down to about 0.5–1.0 ps, pushing the quantum efficiency of emission below 50%. Another non-radiative process activates at elevated temperatures, possibly due to the increased carrier mobility, further halving the observed decay times. For

most materials, a short nonradiative time compared to longer radiative lifetimes would typically result in very efficient luminescence quenching. However, in the case of TMDs with fast radiative times, such as $MoSe_2$, luminescence can still be measured and utilized in ultra-fast optoelectronics, even in the presence of rapid radiative recombination.

Data availability statement

The data that support the findings of this study are openly available at the following URL/DOI: https://doi.org/10.6084/m9.figshare.25093712.

Acknowledgment

This work was supported by National Science Centre, Poland, under Projects 2021/41/N/ST3/04240 and 2021/41/B/ST3/04183. K W and T T acknowledge support from the JSPS KAKENHI (Grant Numbers 21H05233 and 23H02052) and World Premier International Research Center Initiative (WPI), MEXT, Japan. The work has also been supported by the EU Graphene Flagship project. The Polish participation in the European Magnetic Field Laboratory (EMFL) is supported by the DIR/WK/2018/07 grant from the Ministry of Science and Higher Education, Poland. We express our gratitude to Rafał Bożek for measuring the AFM images presented in the Supplementary Information.

Author contributions

K O, A R, T K, and M R conducted photoluminescence and reflectivity measurements. A R analyzed the reflectivity measurements, and K O analyzed all other experimental data. W P and K N prepared the samples. T T and K W produced hBN used in the samples. M P and P K conceived and supervised the project. K O led the preparation of the manuscript, while other authors actively contributed.

Conflict of interest

The authors declare no competing interests.

ORCID iDs

Kacper Oreszczuk https://orcid.org/0000-0001-8830-0005
Wojciech Pacuski https://orcid.org/0000-0001-8329-5278
Aleksander Rodek https://orcid.org/0000-0002-0263-3122
Mateusz Raczyński https://orcid.org/0000-0003-0443-1943
Tomasz Kazimierczuk https://orcid.org/0000-0001-6545-4167
Kenji Watanabe https://orcid.org/0000-0003-3701-8119
Piotr Kossacki https://orcid.org/0000-0002-7558-1044

References

[1] You Y, Zhang X-X, Berkelbach T C, Hybertsen M S, Reichman D R and Heinz T F 2015 Observation of biexcitons in monolayer WSe_2 *Nat. Phys.* **11** 477
[2] He K, Kumar N, Zhao L, Wang Z, Mak K F, Zhao H and Shan J 2014 Tightly bound excitons in monolayer WSe_2 *Phys. Rev. Lett.* **113** 026803
[3] Ross J S *et al* 2013 Electrical control of neutral and charged excitons in a monolayer semiconductor *Nat. Commun.* **4** 1474
[4] Mak K F, Lee C, Hone J, Shan J and Heinz T F 2010 Atomically thin MoS_2: a new direct-gap semiconductor *Phys. Rev. Lett.* **105** 136805
[5] Splendiani A, Sun L, Zhang Y, Li T, Kim J, Chim C-Y, Galli G and Wang F 2010 Emerging photoluminescence in monolayer MoS_2 *Nano Lett.* **10** 1271–5
[6] Zeng H, Dai J, Yao W, Xiao D and Cui X 2012 Valley polarization in MoS_2 monolayers by optical pumping *Nat. Nanotechnol.* **7** 490
[7] Mak K F, He K, Shan J and Heinz T F 2012 Control of valley polarization in monolayer MoS_2 by optical helicity *Nat. Nanotechnol.* **7** 494
[8] Novoselov K S, Jiang D, Schedin F, Booth T J, Khotkevich V V, Morozov S V and Geim A K 2005 Two-dimensional atomic crystals *Proc. Natl Acad. Sci.* **102** 10451–3
[9] Cadiz F *et al* 2017 Excitonic linewidth approaching the homogeneous limit in MoS_2-based van der Waals heterostructures *Phys. Rev.* X **7** 021026
[10] Ajayi O A *et al* 2017 Approaching the intrinsic photoluminescence linewidth in transition metal dichalcogenide monolayers *2D Mater.* **4** 031011
[11] Wierzbowski J *et al* 2017 Direct exciton emission from atomically thin transition metal dichalcogenide heterostructures near the lifetime limit *Sci. Rep.* **7** 12383
[12] Roy A, Movva H C P, Satpati B, Kim K, Dey R, Rai A, Pramanik T, Guchhait S, Tutuc E and Banerjee S K 2016 Structural and electrical properties of $MoTe_2$ and $MoSe_2$ grown by molecular beam epitaxy *ACS Appl. Mater. Interfaces* **8** 7396–402
[13] Fu D *et al* 2017 Molecular beam epitaxy of highly crystalline monolayer molybdenum disulfide on hexagonal boron nitride *J. Am. Chem. Soc.* **139** 9392–400
[14] Chen M-W *et al* 2017 Highly oriented atomically thin ambipolar $MoSe_2$ grown by molecular beam epitaxy *ACS Nano* **11** 6355–61
[15] Pacuski W *et al* 2020 Narrow excitonic lines and large-scale homogeneity of transition-metal dichalcogenide monolayers grown by molecular beam epitaxy on hexagonal boron nitride *Nano Lett.* **20** 3058–66
[16] Wang K *et al* 2013 Ultrafast saturable absorption of two-dimensional MoS_2 nanosheets *ACS Nano* **7** 9260–7
[17] Nie Z, Long R, Sun L, Huang C-C, Zhang J, Xiong Q, Hewak D W, Shen Z, Prezhdo O V and Loh Z-H 2014 Ultrafast carrier thermalization and cooling dynamics in few-layer MoS_2 *ACS Nano* **8** 10931–40
[18] Vega-Mayoral V *et al* 2016 Exciton and charge carrier dynamics in few-layer WS_2 *Nanoscale* **8** 5428–34
[19] Rodek A *et al* 2021 Local field effects in ultrafast light–matter interaction measured by pump-probe spectroscopy of monolayer $MoSe_2$ *Nanophotonics* **10** 2717–28
[20] Połczyńska K E, Denmat S L, Taniguchi T, Watanabe K, Potemski M, Kossacki P, Pacuski W and Kasprzak J 2023 Coherent imaging and dynamics of excitons in $MoSe_2$ monolayers epitaxially grown on hexagonal boron nitride *Nanoscale* **15** 6941–6
[21] Rodek A, Oreszczuk K, Kazimierczuk T, Howarth J, Taniguchi T, Watanabe K, Potemski M and Kossacki P 2024

Interactions and ultrafast dynamics of exciton complexes in a monolayer semiconductor with electron gas *Nanophotonics* **13** 487–97
[22] You J W, Bongu S R, Bao Q and Panoiu N C 2019 Nonlinear optical properties and applications of 2D materials: theoretical and experimental aspects *Nanophotonics* **8** 63–97
[23] Zeng Z, Wang Y, Pan A and Wang X 2023 Ultrafast photocurrent detection in low-dimensional materials *Phys. Status Solidi (RRL)* **18** 2300120
[24] Ludwiczak K *et al* 2021 Heteroepitaxial growth of high optical quality, wafer-scale van der Waals heterostrucutres *ACS Appl. Mater. Interfaces* **13** 47904–11
[25] Liu H, Li Y, You Y S, Ghimire S, Heinz T F and Reis D A 2017 High-harmonic generation from an atomically thin semiconductor *Nat. Phys.* **13** 262–5
[26] Yu H, Talukdar D, Xu W, Khurgin J B and Xiong Q 2015 Charge-induced second-harmonic generation in bilayer WSe_2 *Nano Lett.* **15** 5653–7
[27] Zhang L, Huang Y, Zhu L, Yao Z, Zhao Q, Du W, He Y and Xu X 2019 Polarized THz emission from in-plane dipoles in monolayer tungsten disulfide by linear and circular optical rectification *Adv. Opt. Mater.* **7** 1801314
[28] Bahk Y-M, Ramakrishnan G, Choi J, Song H, Choi G, Kim Y H, Ahn K J, Kim D-S and Planken P C M 2014 Plasmon enhanced terahertz emission from single layer graphene *ACS Nano* **8** 9089–96
[29] Chen H, Corboliou V, Solntsev A S, Choi D-Y, Vincenti M A, de Ceglia D, de Angelis C, Lu Y and Neshev D N 2017 Enhanced second-harmonic generation from two-dimensional $MoSe_2$ on a silicon waveguide *Light Sci. Appl.* **6** e17 060–e17 060
[30] Oreszczuk K, Slawinska J, Rodek A, Potemski M, Skierbiszewski C and Kossacki P 2022 Hybrid electroluminescent devices composed of (In,Ga)N micro-LEDs and monolayers of transition metal dichalcogenides *Nanoscale* **14** 17271–76
[31] Kucharek J, Bożek R and Pacuski W 2023 Molecular beam epitaxy growth of transition metal dichalcogenide (Mo,Mn)Se2 on 2D, 3D and polycrystalline substrates *Mater. Sci. Semicond. Process.* **163** 107550
[32] von der Linde D, Kuhl J and Rosengart E 1981 Picosecond correlation effects in the hot luminescence of GaAs *J. Lumin.* **24–25** 675–8
[33] Rosen D, Doukas A G, Budansky Y, Katz A and Alfano R R 1981 Time resolved luminescence of photoexcited p-type gallium arsenide by population mixing *Appl. Phys. Lett.* **39** 935–7
[34] Wang G, Palleau E, Amand T, Tongay S, Marie X and Urbaszek B 2015 Polarization and time-resolved photoluminescence spectroscopy of excitons in $MoSe_2$ monolayers *Appl. Phys. Lett.* **106** 112101
[35] Fang H H *et al* 2019 Control of the exciton radiative lifetime in van der Waals heterostructures *Phys. Rev. Lett.* **123** 067401
[36] Poh S M *et al* 2018 Molecular beam epitaxy of highly crystalline $MoSe_2$ on hexagonal boron nitride *ACS Nano* **12** 7562–70
[37] Hong J *et al* 2015 Exploring atomic defects in molybdenum disulphide monolayers *Nat. Commun.* **6** 6293
[38] Kumar N, Cui Q, Ceballos F, He D, Wang Y and Zhao H 2014 Exciton diffusion in monolayer and bulk $MoSe_2$ *Nanoscale* **6** 4915–9